Journal of Solid State Chemistry **144,** 68–80 (1999)
Article ID jssc.1998.8119, available online at http://www.idealibrary.com on IDEAL®

Potassium Lanthanum Nitrate System: Phase Equilibria and Thermal and Structural Properties

Anne-Elisabeth Gobichon, Jean-Paul Auffrédic, and Daniel Louër

Laboratoire de Chimie du Solide et Inorganique Moléculaire (UMR 6511 CNRS), Groupe de Cristallochimie, Université de Rennes I, Avenue du Général Leclerc, 35042 Rennes cedex, France

Received June 25, 1998; in revised form November 24, 1998; accepted December 7, 1998

The thermal decompositions of $K_2La(NO_3)_5 \cdot 2H_2O$ and $K_3La_2(NO_3)_9$ have been studied under vacuum and under nitrogen by means of temperature-dependent X-ray diffraction and conventional thermal analysis. It is shown that the complexity of the decomposition processes arises from the formation of liquid phases. Interpretation of the complete decomposition scheme demanded the concurrent determination, by differential scanning calorimetry, of the phase relationships in the two binary systems $LaONO_3$–KNO_3 and $K_3La_2(NO_3)_9$–KNO_3. In addition, the crystal structure of $K_3La_2(NO_3)_9$ has been refined from single-crystal diffraction data (cubic symmetry, $a = 13.6607(5)$ Å, space group $P4_132$). In the diagram $LaONO_3$–KNO_3, the definite compound $LaONO_3 \cdot \frac{1}{3} KNO_3$ has been identified. It undergoes a phase transformation at 310°C ($\Delta_{tr}H^0 = 9700$ J mol^{-1}). The X-ray diffraction patterns of the two varieties have been indexed with orthorhombic symmetry, and, from cell dimension analogies, a crystal structure derived from the structure of $LaONO_3$, with species like "KNO_3" located between layers $(LaO)_n^{n+}$, is suggested. A polymorphic variety of $LaONO_3$ has been observed above 167°C. In the phase diagram $K_3La_2(NO_3)_9$–KNO_3 a eutectic has been found at 0.906 and 250°C. The decomposition of $K_2La(NO_3)_5 \cdot 2H_2O$ takes place with the successive occurrence of the mixture of phases [$K_3La_2(NO_3)_9$, KNO_3], the eutectic $K_3La_2(NO_3)_9 \cdot 9.62KNO_3$, the phase $LaONO_3 \cdot \frac{1}{3}KNO_3$ and, surprisingly, the formation of cubic La_2O_3, which in turn transforms into the hexagonal variety at higher temperature. The decomposition of $K_3La_2(NO_3)_9$ proceeds through the successive formation of $LaONO_3 \cdot \frac{1}{3}KNO_3$ and cubic La_2O_3. From a Rietveld refinement, it has been shown that the crystal structure of cubic La_2O_3 [$a = 11.414(3)$ Å at 540°C] is isostructural with the cubic rate earth sesquioxides. © 1999 Academic Press

Key Words: **potassium lanthanum nitrate; phase diagram; thermal decomposition; structure determination; cubic lanthanum oxide.**

I. INTRODUCTION

The thermal behavior of various solid pentanitrato complexes with the general formula $M^I_2\, Ln^{III}(NO_3)_5 \cdot nH_2O$ (M = alkaline metal, silver, or ammonium ion) has been described in earlier studies (1–6). Their decomposition processes have been found complex and dependent on the experimental conditions used. In particular, a complete interpretation of the thermal decomposition of $Rb_2Ce(NO_3)_5 \cdot 4H_2O$ (1), $(NH_4)_2Ce(NO_3)_5 \cdot 4H_2O$ (5), and $Ag_2Ce(NO_3)_5 \cdot H_2O$ (6), based on the use of temperature-dependent X-ray powder diffraction (TDXD) and conventional thermal analysis, has been reported. All phases formed during the thermal treatment were identified and characterized from X-ray powder diffraction. The lanthanum compound $K_2La(NO_3)_5 \cdot 2H_2O$, known for its nonlinear optical properties with high performance (7), belongs to this family of compounds. Its crystal structure was described by Eriksson *et al.* (8). In a previous study about its thermal decomposition, based on thermogravimetric analysis, formation of the intermediate anhydrous compound $K_2La(NO_3)_5$ and the final mixed oxide $KLaO_2$ was suggested (2). However, a new investigation of the thermal behavior of this compound with TDXD, thermogravimetry (TG), and differential scanning calorimetry (DSC) has revealed that the decomposition scheme is much more complex than previously described. To explain completely the decomposition process of $K_2La(NO_3)_5 \cdot 2H_2O$, it has been necessary to synthesize the related phase $K_3La_2(NO_3)_9$. The crystal structure and the thermal decomposition of the last compound were subsequently studied. Also, the phase relationships in the two binary systems $LaONO_3$–KNO_3 and $K_3La_2(NO_3)_9$–KNO_3 were concurrently determined. Moreover, the interpretation of the results has been greatly facilitated by the detailed information reported recently (9) on the thermal behavior of neutral lanthanum nitrate hexahydrate. The present study deals with a thorough description of the thermal decomposition process of $K_2La(NO_3)_5 \cdot 2H_2O$ and the structural features of the observed phases.

II. EXPERIMENTAL

Materials Preparation

The starting material $K_2La(NO_3)_5 \cdot 2H_2O$ was prepared by slow crystallization, at room temperature, from an

0022-4596/99 $30.00

aqueous solution of KNO_3 (Merck) and $La(NO_3)_3 \cdot 6H_2O$ (Prolabo) in the molar ratio 2:1. Single crystals of $K_2La_2(NO_3)_9$ were obtained from evaporation, at room temperature, of a concentrated nitric acid solution of KNO_3 and $La(NO_3)_3 \cdot 6H_2O$ with the molar ratio 3:2.

Density measurements were carried out with an automatic helium picnometer (AccuPyc 1330, Micromeritics).

X-Ray Diffraction

TDXD measurements were carried out with an INEL (CPS120) curved position sensitive detector, using monochromatic Cu$K\alpha_1$ radiation ($\lambda = 1.5406$ Å) and semi focusing diffraction geometry (10). The sample was deposited on a flat sample holder located in a high-temperature device (Rigaku) designed to maintain the specimen in a controlled atmosphere. An angle of the incident beam with respect to the flat sample of 5° was generally used. Radiation shields located around the sample were used to ensure a homogeneous temperature. One shield in aluminum (0.01 mm thick) was used in experiments up to 600°C, while two shields in nickel (0.005 mm thick) were necessary for studies up to 800°C. These experimental constraints explain the low counting statistics obtained in the higher-temperature studies and, consequently, the lower quality of the corresponding three-dimensional diffraction plots.

Precise X-ray powder diffraction data were collected *ex situ* at room temperature with a D500 Siemens powder diffractometer equipped with an incident-beam germanium monochromator (Cu$K\alpha_1$ radiation). *In situ* diffraction data were also obtained under isothermal conditions with a Siemens diffractometer, using a diffracted-beam graphite monochromator (Cu$K\alpha_{1,2}$ radiation), equipped with a high-temperature attachment. The peak positions were extracted with the pattern decomposition technique, using the fitting program PROFILE from Socabim, available in the software package DIFFRAC-AT supplied by Siemens. Indexing of the powder diffraction patterns was performed with the program DICVOL91 (11).

For the single-crystal study of $K_3La_2(NO_3)_9$, X-ray diffraction data were measured with an Enraf–Nonius CAD-4 diffractometer (Mo$K\alpha$ radiation, $\lambda = 0.710$ Å). A crystal was introduced in a capillary to prevent hydration. One set of intensities ($0 \leq h, k, l \leq 27$) was collected at room temperature by a θ–2θ scanning technique. Data were corrected for Lorentz polarization and extinction effects. Absorption corrections were based on ψ scans. All calculations were carried out with the software package MolEN (12).

Thermal Analysis

TG measurements were carried out under vacuum by means of a McBain-type thermobalance. For TG or simultaneous TG–DSC experiments performed under a nitrogen stream a Thermoflex TG–DSC instrument (Rigaku) was used. When only the TG curve was recorded, a powdered sample of about 50 mg was spread evenly in a large sample holder to avoid mass effect. In the other cases the sample weight was 10–20 mg. The DSC unit was calibrated using reference materials, i.e., indium, tin, lead, potassium nitrate, and potassium perchlorate (13). DSC runs were recorded using aluminum pans with lids. Calcined alumina was used as reference material.

III. CRYSTAL STRUCTURE OF $K_3La_2(NO_3)_9$

The powder diffraction pattern of the phase $K_3La_2(NO_3)_9$ was indexed with a cubic unit cell, with the refined parameter $a = 13.6607(5)$ Å [$V = 2549.3(3)$ Å^3, $M_{20} = 62$, $F_{30} = 97(0.0077,40)$] [PDF File No. 47-0887, ICDD (14)]. This value is close to the unit cell constant of $K_3Ce_2(NO_3)_9$ [$a = 13.597(8)$ Å, $V = 2514.1(4)$ Å^3, space group $P4_132$], whose crystal structure was solved recently (15). Due to the isostructural relationship with the cerium analogue, the atomic coordinates of $K_3Ce_2(NO_3)_9$ were used as initial coordinates in the refinement from single-crystal diffraction data. The R and ωR values, based on 64 refined parameters and 1886 reflections, were 0.027 and 0.035, respectively. The atomic coordinates are given in Table 1. The structure consists of a three-dimensional $[La_2(NO_3)_9]^{3-}$ network of irregular icosahedra formed by oxygen atoms from bidentate nitrate groups. These polyhedra are linked together through bridging nitrate groups [see Fig. 2 in Ref. (15)] The La–O distances are in the range 2.614(3)–2.778(3) Å, with the average value 2.676 Å. This value is in a good agreement with the results reported for similar polyhedra in some compounds, e.g., $La_2Mg_3(NO_3)_{12} \cdot 24H_2O$ (2.642–2.696 Å, average 2.670 Å) (16), $LaAl(NO_3)_6 \cdot 12H_2O$ and $LaAl(NO_3)_6 \cdot 6H_2O$ (2.628–2.679 Å, average 2.652 and 2.660 Å, respectively) (17), and $Li_3La_2(NO_3)_9 \cdot 3H_2O$ (2.580–2.718 Å, average 2.655 Å) (18). The K atoms are located in the holes of the structure.

TABLE 1
Atomic Coordinats and Atomic Displacement Parameters for $K_3La_2(NO_3)_9$

Atom	x	y	z	B_{iso}(Å^2)
La	0.54817(1)[a]	0.54817(1)	0.54817(1)	1.41(1)
K	0.125	− 0.18675(6)	0.0632(6)	2.93(1)
N1	0.1100(2)	0.3387(2)	0.3514(2)	2.36(5)
O11	0.1892(2)	0.3611(2)	0.3073(2)	2.64(4)
O12	0.1760(2)	0.0836(2)	0.5058(2)	2.78(5)
O13	0.1577(2)	0.6464(2)	0.1795(2)	4.12(6)
N2	0.125	− 0.0127(2)	0.2373(2)	1.68(4)
O21	0.125	0.0543(2)	0.3043(2)	1.89(3)
O22	0.8445(2)	0.6571(2)	0.4911(2)	2.28(4)

[a] SD in parentheses.

IV. THERMAL DECOMPOSITION OF $K_2La(NO_3)_5 \cdot 2H_2O$

Thermal Decomposition under Vacuum

The TG curve shown in Fig. 1 (curve *a*) suggests that the decomposition proceeds through two stages. On the contrary, the three-dimensional (3D) plot of the changes with temperature of the powder diffraction patterns (Fig. 2) shows that the decomposition is much more complex.

In a first stage, between 40 and 90°C, the experimental weight loss (6.27%) is in good agreement with the total dehydration of the precursor (theoretical value 6.39%), which suggests the formation of $K_2La(NO_3)_5$. Nevertheless, at the end of this stage the powder diffraction patterns observed in Fig. 2 show that the solid obtained is in fact $K_3La_2(NO_3)_9$. It must be noted that the diffraction lines are very broad below $\sim$100°C. In addition, the polymorphic variety of potassium nitrate, β-KNO_3 (strongest line at 26.20°2θ), can clearly be identified above 128°C, which is the transition temperature between α- and β-KNO_3. Consequently, it can be concluded that KNO_3 is also a decomposition product of the precursor. This feature means that, below 128°C, KNO_3 is amorphous or highly divided, since no diffraction lines are observed in the 3D plot. It should be noted that the formation of such an amorphous single nitrate, i.e., $RbNO_3$, has already been reported in the thermal decomposition of $CeRb_2(NO_3)_5$ (1). From these observations, the first decomposition stage may be written.

$$2K_2La(NO_3)_5 \cdot 2H_2O \rightarrow K_3La_2(NO_3)_9 + KNO_{3(am)} + 4H_2O, \quad [1]$$

which, similarly to the formation of $K_2La(NO_3)_5$, corresponds fortuitously to a theoretical weight loss of 6.39%.

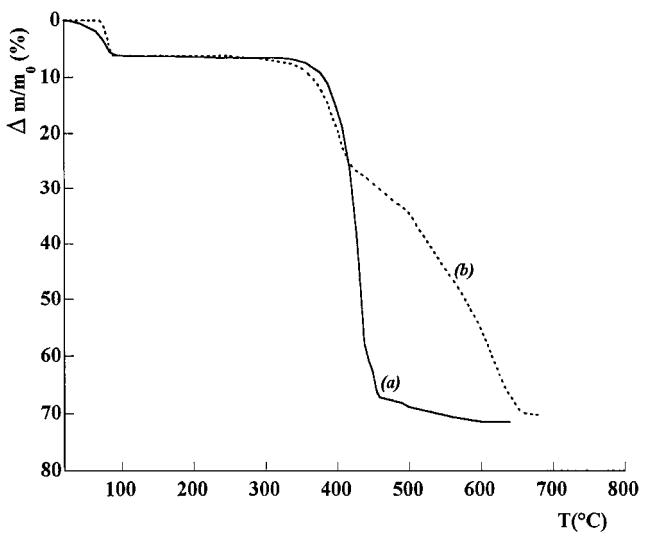

FIG. 1. TG curves for the thermal decomposition of $K_2La(NO_3)_5 \cdot 2H_2O$ under vacuum (a) and under nitrogen (b) (heating rate: 10°C h^{-1}).

In a second stage, above 250°C, a new phase denoted X_α appears, while the X-ray diffraction lines of β-KNO_3 and $K_3La_2(NO_3)_9$ vanish (see Fig. 2). At about 350°C, a sudden subtle shift of a few diffraction lines (e.g., the line at 28.04°2θ) of X_α is observed. This feature suggests that X_α undergoes a phase transformation into a polymorphic modification, denoted X_β. These phases are discussed further below. During these transformations there is no weight loss (Fig. 1a).

Above 370°C, the TG curve exhibits a rapid sample weight loss up to 450°C. The final weight loss (72.0%), achieved only above 650°C, is in good agreement with the formation of pure lanthanum oxide La_2O_3 (theoretical: 71.07%). This result was confirmed by the chemical analysis of the residue, based on energy-dispersive spectrometry (ESD). Surprisingly, the diffraction patterns observed in the range 450–650°C do not correspond to hexagonal La_2O_3, which is the stable phase known for lanthanum oxide. Therefore, it must be concluded that a polymorph of lanthanum oxide is formed during the thermal decomposition under vacuum of $K_2La(NO_3)_5 \cdot 2H_2O$. This phase was easily identified as isostructural with the cubic rare earth sesquioxides. This unexpected result is discussed in more detail in Section IX. This metastable phase transforms in turn partially above 650°C into the hexagonal variety (Fig. 2).

Thermal Decomposition under Nitrogen

Figure 3 shows that, under a nitrogen stream, the overall decomposition scheme of the precursor is similar to that described under vacuum, except that cubic La_2O_3 is observed only in a short temperature range (470–520°C) and its transformation into hexagonal La_2O_3 is complete above 530°C. Also, it should be noted that the X phases are better crystallized, even though the first line (002 at $\sim$7.3°2θ) is not observed because a greater incident angle ($\sim$7°) of the incident beam on the stationary flat sample was used in this experiment. The TG curve (Fig. 1b) compares well with that reported by Karppinen *et al.* (2). The inflection point observed at about 420°C and the slow weight loss in the range 420–650°C can be explained by a slow desorption, from highly divided La_2O_3, of the gaseous decomposition products formed above 420°C. It should be noted that the TDXD plot (Fig. 3) does not display the formation of the mixed oxide $KLaO_2$ as reported previously (2).

Moreover, Fig. 3 shows that the intensity of the diffraction lines of $K_3La_2(NO_3)_9$ decreases suddenly at about 250°C (see the more intense lines) and that the lines of β-KNO_3 vanish (e.g., line at 26.20°2θ). To explain this feature, simultaneous TG and DSC studies of the precursor were carried out in the temperature range 20–300°C. The DSC curve in Fig. 4a displays a large peak which is

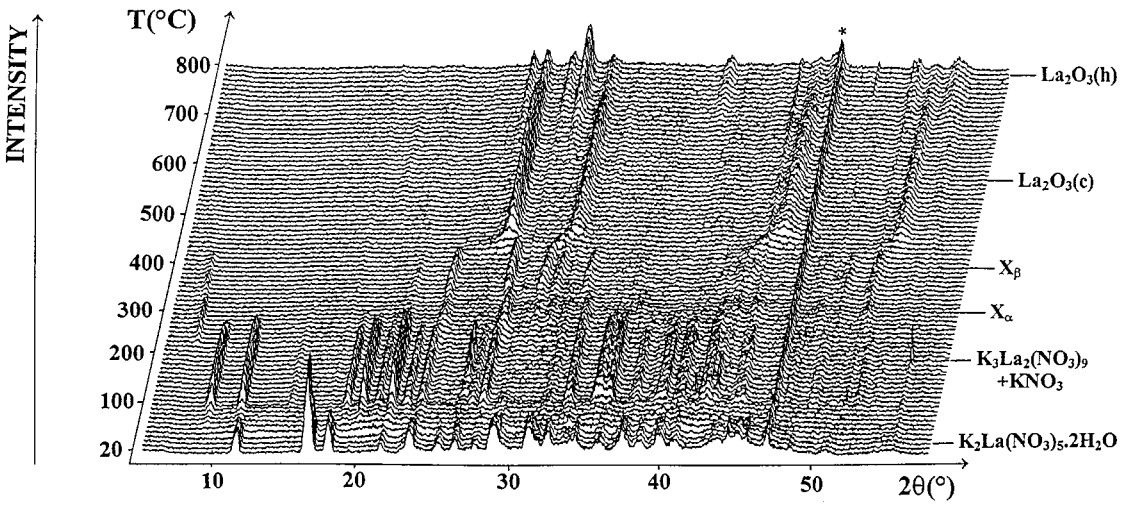

FIG. 2. TDXD plot for $K_2La(NO_3)_5 \cdot 2H_2O$ under vacuum (heating rate: 20°C h^{-1}; counting time for each pattern: 1800 s; ∗: diffraction line from the sample holder; c: cubic; h:hexagonal).

associated with the decomposition of the precursor. A second sharp peak is observed at 250°C, while the TG curve (Fig. 4b) exhibits only a plateau from 100°C. This thermal effect suggests the occurrence of a "phase transformation" at 250°C under nitrogen, which is reversible since an exothermic peak was observed on cooling. It should be noted that no thermal effect due to the recrystallization of amorphous KNO_3 into β-KNO_3 was observed.

At this stage two main aspects of the decomposition remain unexplained, i.e., the apparent "phase transformation" of $K_2La_2(NO_3)_9$ observed at 250°C and the nature of the phases denoted X. To further interpret the decomposition process, the thermal behavior of pure $K_3La_2(NO_3)_9$ has been investigated independently.

V. THERMAL DECOMPOSITION OF $K_3La_2(NO_3)_9$

Although $K_3La_2(NO_3)_9$ is air sensitive, crystals could be ground and used for a TDXD experiment carried out under vacuum (Fig. 5). Some line intensity variations are observed in the temperature range where the phase is thermally stable. This is related to slight changes, occurring during heating, of the orientation of the anisotropic crystallites in the stationary sample. This geometry-diffraction-dependent effect has already been discussed in detail elsewhere (10). However, it is clear that the decomposition of the pure phase $K_3La_2(NO_3)_9$ up to 600°C takes place with the successive formation of X_α, X_β, and also cubic La_2O_3. The corresponding TG curve (Fig. 6) shows that the weight loss

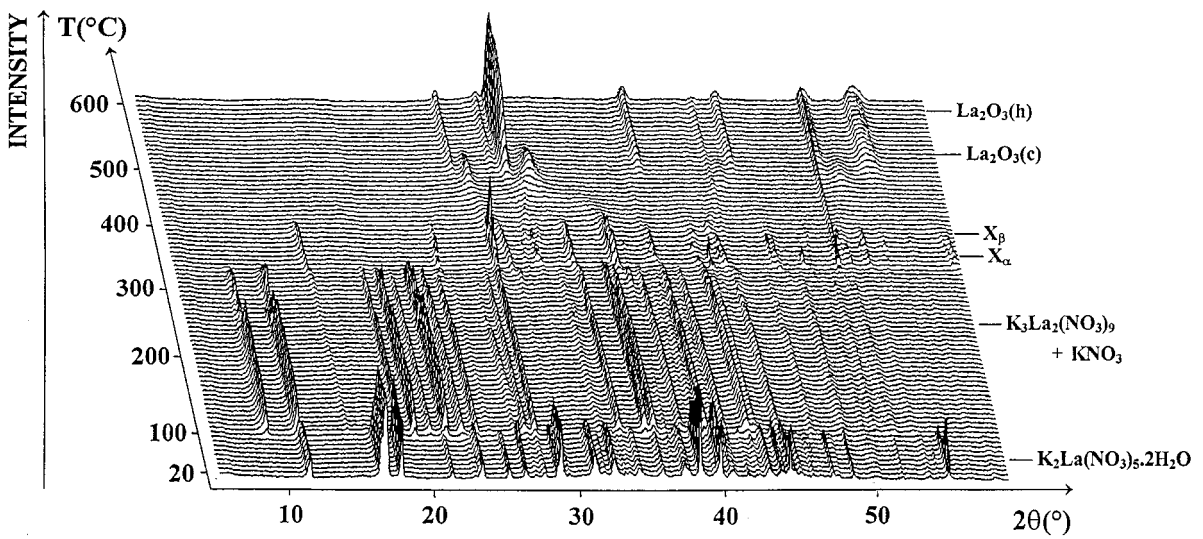

FIG. 3. TDXD plot for $K_2La(NO_3)_5 \cdot 2H_2O$ under nitrogen (heating rate: 10°C h^{-1}; counting time for each pattern: 2700 s; c: cubic; h: hexagonal).

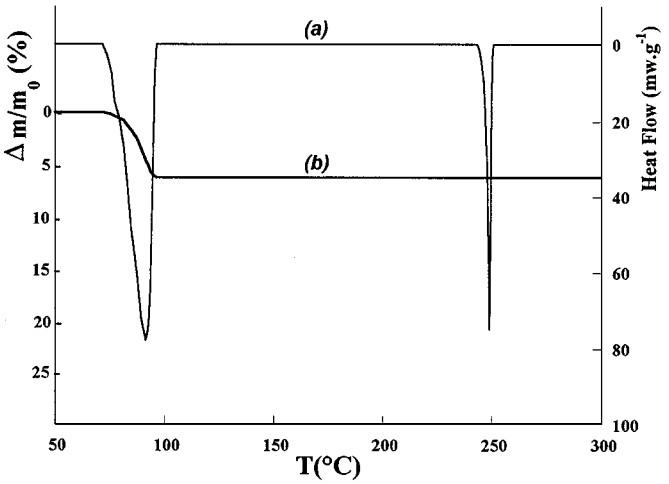

FIG. 4. DSC (a) and TG (b) curves for the decomposition of $K_2La(NO_3)_5 \cdot 2H_2O$ under nitrogen (heating rate: 20°C h^{-1}).

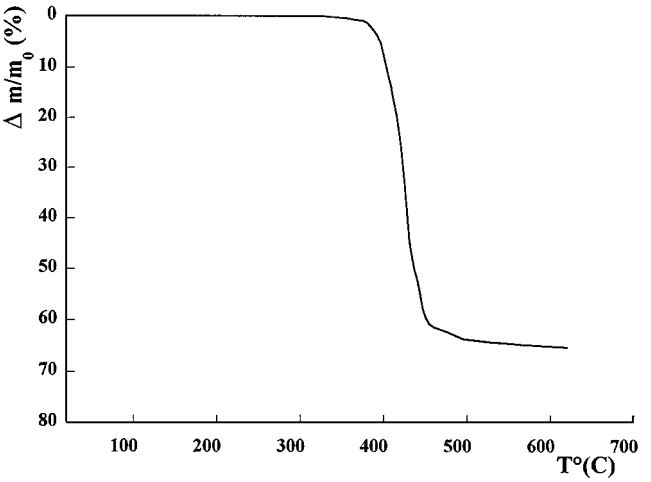

FIG. 6. TG curve for the thermal decomposition of $K_3La_2(NO_3)_9$ under vacuum (heating rate: 5°C h^{-1}).

occurs in a single stage and is delayed with regard to the transformation of the precursor into X_α, as seen in Fig. 5. The weight loss (65.0%) on completion agrees well with the final formation of pure La_2O_3 (theoretical: 65.08%).

With respect to Fig. 3, no sudden intensity change of the diffraction lines of $K_3La_2(NO_3)_9$ is observed at 250°C. This results demonstrates tht the "phase transformation" suggested in the previous section takes place only if $K_3La_2(NO_3)_9$ is mixed with β-KNO_3. To explain this problem the phase relationships in the binary system $K_3La_2(NO_3)_9$–KNO_3 have been determined. They are described in Section VIII.

Moreover, to elucidate the nature of the phases denoted X, powder diffraction data of a quenched decomposition product prepared at 350°C were collected at room temperature. Surprisingly, they revealed the presence of a mixture of X_α and α-KNO_3. This result means that the decomposition of $K_3La_2(NO_3)_9$ proceeds through the simultaneous formation of X_α and KNO_3, which becomes liquid at 334°C. The absence of the diffraction lines of β-KNO_3 (Fig. 5) in the temperature range 220–334°C can again be explained by the fact that KNO_3 formed during the thermal decomposition is amorphous.

VI. CHARACTERIZATION OF X_α AND X_β

The crystallographic data of X_α were extracted from precise powder diffraction data (Fig. 7). The pattern was

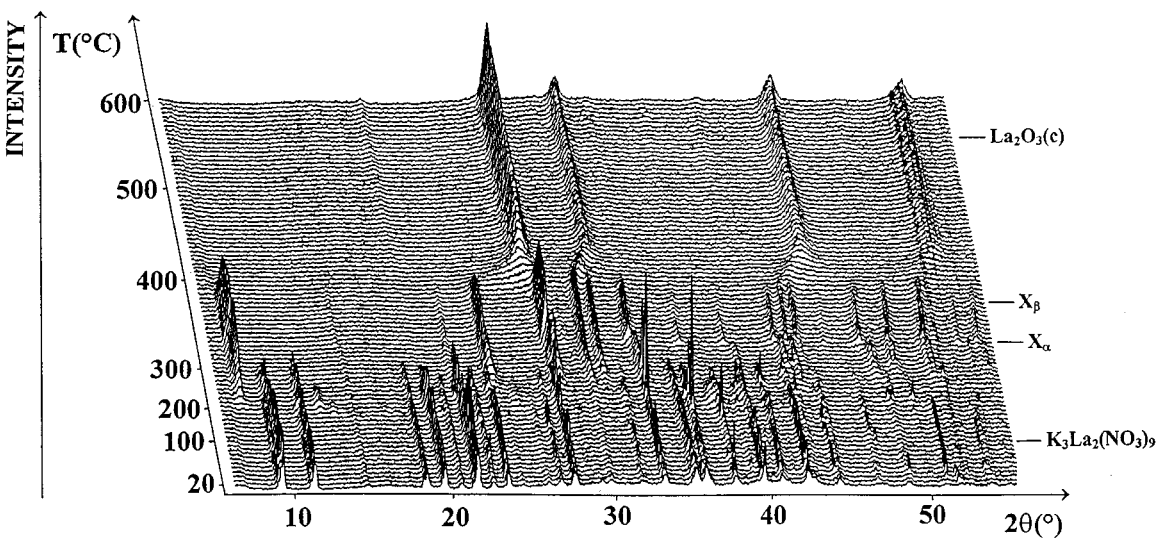

FIG. 5. TDXD plot for $K_3La_2(NO_3)_9$ under vacuum (heating rate: 20°C h^{-1} in the range 20–300°C, 10°C h^{-1} in the range 300–600°C; counting time for each pattern: 1800 s; c: cubic).

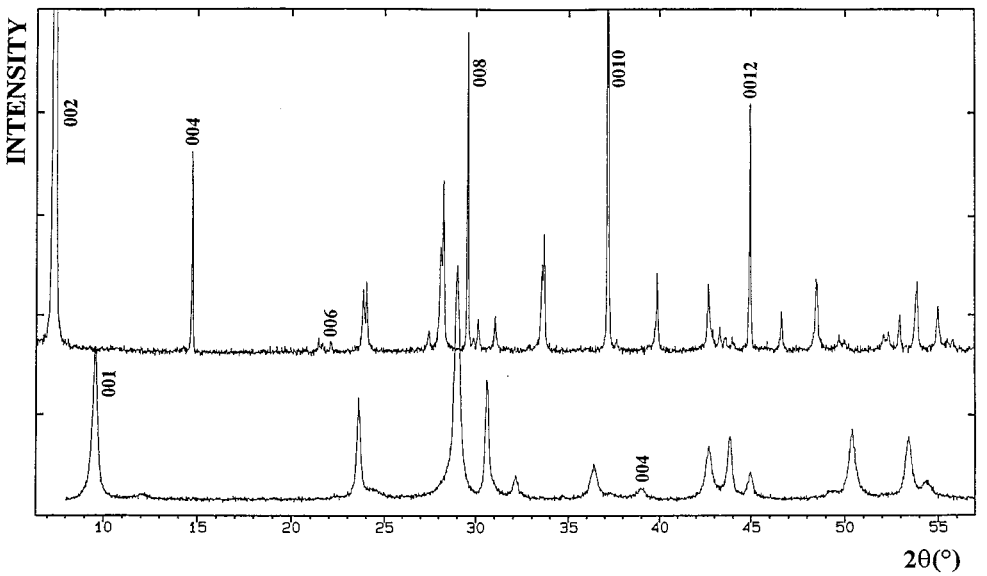

FIG. 7. Powder diffraction patterns of (top) X_α ($LaNO_3 \cdot \frac{1}{3} KNO_3$, see Section VII) and (bottom) $LaONO_3$ (variety α, see Section VII).

indexed with an orthorhombic unit cell and data were reviewed with the program NBS*AIDS83 (19). The systematic absent reflections were found in accordance with an *I*-centered lattice. The refined parameters and figures of merit, calculated for allowed reflections, are $a = 4.1818(5)$ Å, $b = 4.2188(7)$ Å, $c = 24.223(2)$ Å, $V = 427.34(7)$ Å^3, $M_{20} = 57$, and $F_{30} = 59(0.0111,46)$. For X_β the powder diffraction data were collected *in situ* under nitrogen at 390°C. The pattern was also indexed with an orthorhombic unit cell. The refined parameters and figures of merit, calculated from allowed reflections, are $a = 4.1819(7)$ Å, $b = 4.2365(7)$ Å, $c = 24.467(3)$ Å, $V = 433.47(9)$ Å^3, $M_{20} = 104$, and $F_{30} = 69(0.0101,43)$. The powder data have been submitted to the ICDD (14) for possible inclusion in the Powder Diffraction File.

From the interrogation of the NIST CDF database (20) no isostructural chemically related material was found. However, it can be noted that the diffraction patterns of the two phases present some similarities with that of tetragonal $LaONO_3$ [$a = 4.127(4)$ Å, $c = 9.239(1)$ Å, $V = 157.38(3)$ Å^3] (9), which has a layer structure closely related to the matlockite (PbFCl)-type structure. The parameters *a* and *b* of X_α and X_β compare well with the parameter *a* of $LaONO_3$, while parameters *c* are much greater than the interlayer spacing in the structure of $LaONO_3$. Consequently, it can be expected than the structures of X_α and X_β are likely derived from that of $LaONO_3$, with some "unidentified species" located between the layers. This comment is also supported by the shift of the 00*l* reflections of X_α toward lower angles, with respect to the 00*l* reflections of $LaONO_3$ (Fig. 7). Moreover, since $K_3La_2(NO_3)_9$ decomposes into X_α and KNO_3, it can be thought that KNO_3 is involved in the formation of X_α. To further support this suggestion, the phase relationships in the binary system $LaONO_3$–KNO_3 have been investigated in detail.

VII. PHASE EQUILIBRIA IN THE SYSTEM $LaONO_3$–KNO_3

Mixtures of KNO_3 and $La(NO_3)_3 \cdot 6H_2O$ with different molar ratios *x* ($0 < x < 0.7$) were heated in air at 400°C. At this temperature, the mixtures are liquid and decompose partially. After 1 h, a solid was obtained and thus quenched at room temperature. From the total observed weight loss, its global composition can be written as $LaONO_3 \cdot xKNO_3$. From the analysis of the powder diffraction patterns, the solids formed were identified in the quenched samples, i.e.,

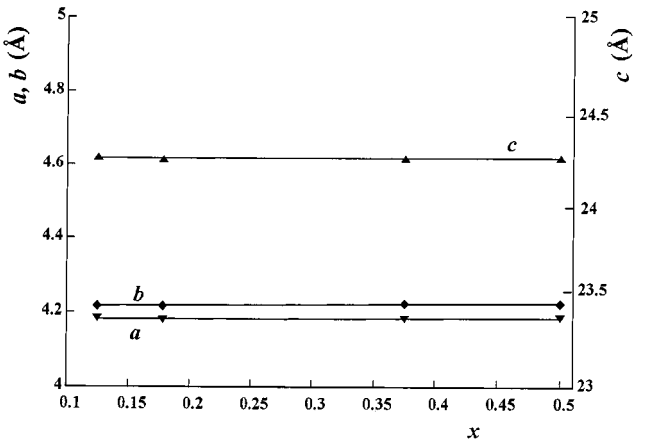

FIG. 8. Unit cell parameters of X_α versus the molar ratio $x(KNO_3/LaONO_3)$.

$LaONO_3$ for $x = 0$, a mixture of $LaONO_3$ and X_α for $0 < x \leq 0.30$, and a mixture of X_α and α-KNO_3 for $x > 0.35$.

Figure 8 displays the unit cell parameters of X_α as a function of x ($0.1 < x < 0.50$). It shows that the parameters a, b, and c are not dependent on x. This result means that X_α is not a solid solution of KNO_3 and $LaONO_3$, but is a definite compound. This analysis gives evidence that KNO_3 is necessarily a constituent of the phase X_α. Consequently, if $LaONO_3 \cdot yKNO_3$ is the chemical formula of X_α, the synthesis reactions can be written, for $0 < x \leq 0.3$,

$$La(NO_3)_3 \cdot 6H_2O + xKNO_3 \rightarrow (x/y)(LaONO_3 \cdot yKNO_3) + (1 - x/y)LaONO_3 + (NO, NO_2, O_2, 6H_2O), \quad [2]$$

and for $x > 0.35$,

$$La(NO_3)_3 \cdot 6H_2O + xKNO_3 \rightarrow (LaONO_3 \cdot yKNO_3) + (x - y)KNO_3 + (NO, NO_2, O_2, 6H_2O). \quad [3]$$

Representative DSC curves recorded in the temperature range 40–400°C from samples of global composition $LaONO_3$, $xKNO_3$, for which $x = 0$, $x = 0.25$, and $x = 0.50$ are displayed in Fig. 9 (curves *a*, *b*, and *c*, *d*, respectively). They show endothermic peaks whose number depends on the value of x. They can be clearly ascribed to phase transformations since no weight loss was detected on the TG curves recorded simultaneously. Additional features worthy of comments are as follows:

$x = 0$. Only one thermal event is observed in the range 165–180°C (Fig. 9a). It corresponds to the transformation of $LaONO_3$ from a low-temperature phase, denoted α-$LaONO_3$, to a high-temperature phase (β-$LaONO_3$). The heat change for this transformation was measured as 2940(40) J mol^{-1}. The diffraction pattern of β-$LaONO_3$, obtained *in situ* at 180°C, was indexed with a tetragonal unit cell. The refined parameters and figures of merit, calculated for allowed reflections in space group $P4/nmm$, are $a = 4.1636(2)$ Å, $c = 9.3979(6)$ Å, $V = 162.92(2)$ Å^3, $M_{20} = 117$, and $F_{28} = 92(0.0083,37)$. These parameters are slightly elongated by about 0.87 and 1.87% with respect to those reported for α-$LaONO_3$ [$a = 4.127(4)$ Å, $c = 9.239(1)$ Å] (9).

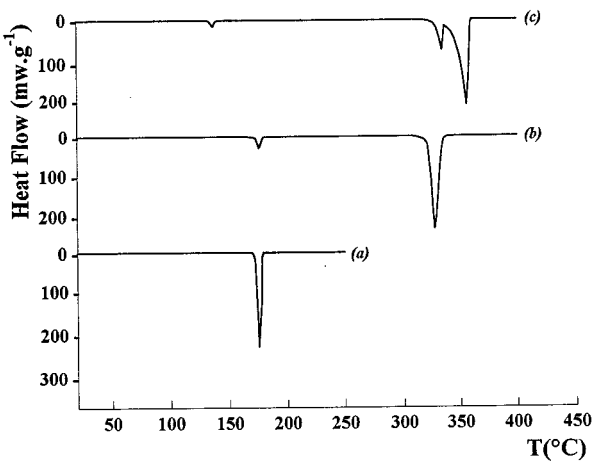

FIG. 9. DSC curves for samples $LaONO_3 \cdot xKNO_3$ under nitrogen (heating rate: 200°C h^{-1}). (a) $x = 0$, (b) $x = 0.25$, (c) $x = 0.5$.

$x = 0.25$. The DSC curve displayed in Fig. 9b is representative of samples for which x is in the range 0–0.30. In addition to the peak observed for $x = 0$, a second peak is displayed between 310 and 340°C. From TDXD it was concluded that this thermal event is due to the phase transformation of X_α into X_β. Moreover, from the DSC measurements of the heat of this phase transformation performed from various samples, it was possible to check the validity of reaction [2]. Indeed, according to the stoichiometric coefficient of the reaction, the heat of the phase transformation X_α–X_β for a mixture (X_α, $LaONO_3$) is given by

$$Q = (n_1/y)\ \Delta_{tr}H^\circ, \quad [4]$$

where n_1 is the amount of KNO_3 in the sample, y the number of moles of "KNO_3" in the formula unit of the new compound X_α, and $\Delta_{tr}H^\circ$ the enthalpy change for the phase transformation X_α–X_β. Consequently, the ratio Q/n_1 must be constant for x ranging from 0 to 0.30. The experimental values of Q/n_1 for various samples are given in Table 2. It is seen that Q/n_1 is almost constant with the average value 29520(160) J mol^{-1}. This result demonstrates that chemical reaction [2] is correct.

$x = 0.50$. Three endothermic peaks are observed on the DSC curve (Fig. 9c). The first one, between 130 and 140°C, is due to the phase transformation α–β of KNO_3 (13). In the temperature range 310–360°C, two peaks overlap. The first one was identified as the melting of β-KNO_3 (melting point: 334°C) and the second one was explained from TDXD as the phase transformation of X_α into X_β. It can be seen that

TABLE 2
Experimental Heat Q of the Phase Transformation X_α–X_β for Various Mixtures ($LaONO_3$, $xKNO_3$)

x	m^a (mg)	$n_1 \times 10^5$ (mol)	Q (J)	Q/n_1 (kJ mol^{-1})	y
0.10	28.98	1.276	0.381	29.86	0.325
0.125	31.30	1.704	0.554	32.51	0.298
0.167	36.18	2.585	0.706	27.31	0.356
0.20	30.47	2.570	0.744	28.95	0.335
0.25	30.35	3.133	0.929	29.65	0.328
0.30	32.05	3.888	1.123	28.88	0.336

[a] m, sample mass; n_1, number of moles of KNO_3 in sample.

the peak tip is at 357°C, instead of 317°C observed for an x value in the range 0–0.30. It is likely that the concomitant melting of KNO_3 in excess induces a change in the transformation kinetics. According to the stoichiometric coefficients in reaction [3] the amount of X_α in a mixture (X_α, KNO_3) is equal to that of "$LaONO_3$." Consequently, $\Delta_{tr}H^0$ can be calculated from the heat measured from the DSC runs. Several DSC measurements were performed with different mixtures ($LaONO_3$, KNO_3) with values of x in the range 0.4–0.9. The calculated mean value of $\Delta_{tr}H^0$ was 9700(130) J mol^{-1}. Then, from Eq. [4] and the experimental heats Q obtained for samples with different compositions x, given in Table 2, the values of y were calculated and are listed in the last column of Table 2. It can be seen that y is almost constant. Its average value was calculated as 0.33(2). This specific value indicates that the chemical formula of X_α must be $LaONO_3 \cdot \frac{1}{3} KNO_3$.

In addition, from all these results the phase diagram of the binary system $LaONO_3$–$xKNO_3$ ($0 < x < 1$) could be established in the temperature range 20–400°C (Fig. 10). It should be noted that $LaONO_3 \cdot \frac{1}{3}KNO_3$ was also obtained independently from a stoichiometric mixture of $LaONO_3$ and KNO_3, heated at 400°C for about 1 h and subsequently quenched at room temperature. This result indicates that this phase is the product of a peritectic reaction between a liquid rich in KNO_3 and β-$LaONO_3$, occurring at a temperature that could not be determined. On the other hand, though a small amount of an impurity phase (KNO_3) was often observed in the sample, the density of $LaONO_3 \cdot \frac{1}{3}KNO_3$ was measured as 3.64 g cm^{-3}, which agrees satisfactorily with the value calculated from the unit cell dimensions, i.e., 3.84 g cm^{-3} for $Z = 4$.

VIII. THE BINARY SYSTEM $K_3La_2(NO_3)_9$–KNO_3

Samples of $K_3La_2(NO_3)_9$ were prepared from a stoichiometric mixture of $La(NO_3)_3 \cdot 6H_2O$ and KNO_3 heated at 90°C. DSC studies of mixtures [$K_3La_2(NO_3)_9$, KNO_3] with different molar fractions z of KNO_3 ($0.369 < z < 0.975$) were carried out under nitrogen at 200°C h^{-1}. A representative DSC response for a sample with $z = 0.70$ is displayed in Fig. 11. The first peak at 130°C was identified as the transition α–β of KNO_3. The strong endotherm between 245 and 260°C was ascribed to the transformation already observed in the same temperature range during the decomposition under nitrogen of $K_2La(NO_3)_5 \cdot 2H_2O$ (see Fig. 4a). On the other hand, the endothermic peak corresponding to the melting of pure KNO_3 at 324°C was never observed. Similar DSC curves were obtained whatever the composition of the sample studied. Furthermore, a partial melting of the samples occurring on heating at about 250°C was pointed out by optical microscopy. To conclude, it can be stated that these results are consistent with the formation of a eutectic from the solid mixture [$K_3La_2(NO_3)_9$, KNO_3]. Thus, if z_E is the molar fraction of KNO_3 in the eutectic, the eutectic reaction can be written

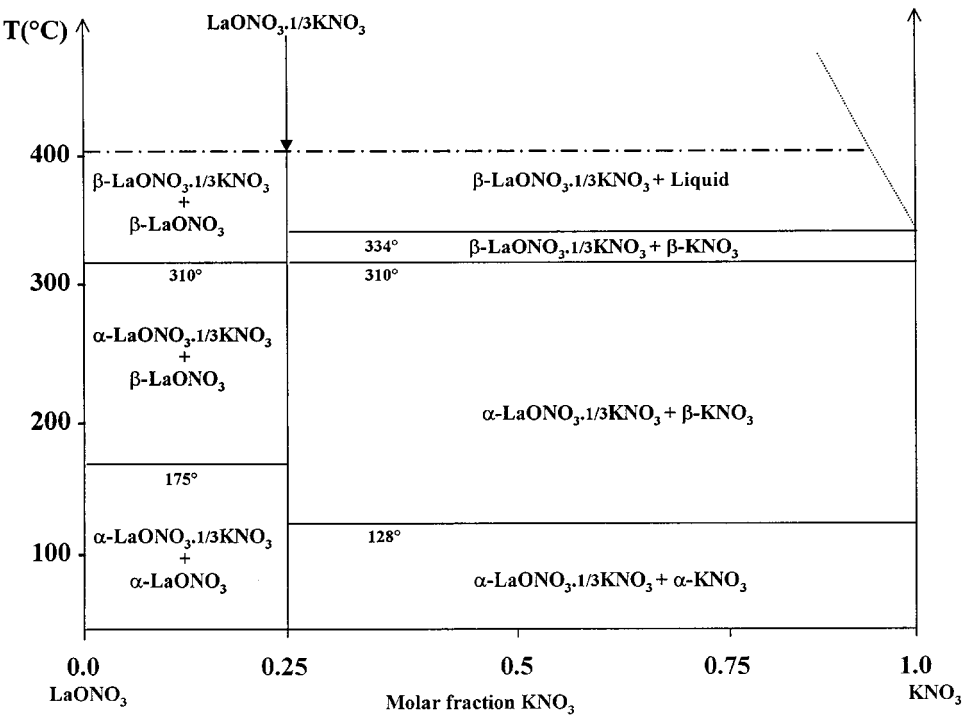

FIG. 10. $LaONO_3$–KNO_3 phase diagram (the dotted line is assumed to be the liquidus border).

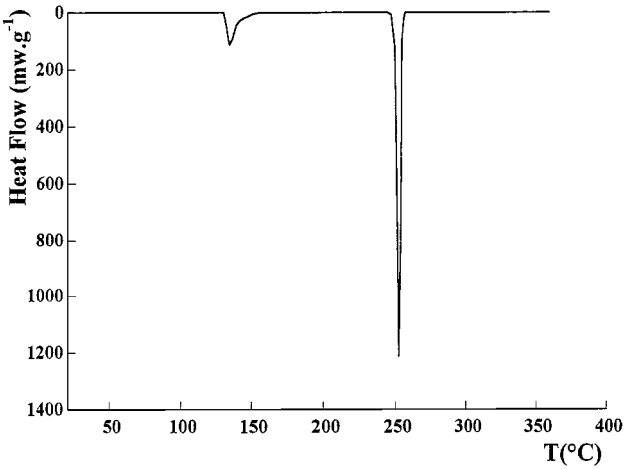

FIG. 11. DSC curve for $K_3La_2(NO_3)_9 \cdot 0.70KNO_3$ under nitrogen (heating rate: 200°C h^{-1}).

TABLE 3
Experimental Heat Q Evolved in Mixtures $[(1-z)K_3La_2(NO_3)_9, zKNO_3]$ at the Eutectic Point

z	m^a (mg)	$n_1 \times 10^5$ (mol)	$n_2 \times 10^5$ (mol)	Q (J)	Q/n_1 (kJ mol^{-1})	Q/n_2 (kJ mol^{-1})
0.369	33.04	1.9110	3.272	0.370	19.34	11.31
0.539	29.47	3.220	2.743	0.630	19.56	22.97
0.700	30.54	6.011	2.569	1.171	19.46	45.54
0.824	33.08	10.870	2.319	2.150	19.78	92.71
0.857	26.17	10.072	1.679	1.98	19.66	117.92
0.909	31.09	15.831	1.583	2.84	17.94	179.41
0.923	28.45	15.760	1.313	2.048	15.74	188.88
0.952	31.24	21.009	1.050	2.02	9.91	192.38
0.975	28.26	22.621	0.565	1.140	4.95	198.23

[a] m, sample mass; n_1, number of moles of KNO_3; n_2, number of moles of $K_3La_2(NO_3)_9$.

for $z < z_E$,

$$(1-z)K_3La_2(NO_3)_9 + zKNO_3 \rightarrow (z/z_E)[(1-z_E)K_3La_2(NO_3)_9 \cdot z_E KNO_3]_{(l)} + (1-z/z_E)K_3La_2(NO_3)_9, \quad [5]$$

and for $z > z_E$,

$$(1-z)K_3La_2(NO_3)_9 + zKNO_3 \rightarrow [(1-z)/(1-z_E)][(1-z_E)K_3La_2(NO_3)_9 \cdot z_E KNO_3]_{(l)} + [(z-z_E)/(1-z_E)]KNO_3. \quad [6]$$

If n_1 is the number of moles of KNO_3 and n_2 that of $K_3La_2(NO_3)_9$ in the initial mixture, the amount of formed eutectic calculated from these last equations is n_1/z_E for $z < z_E$ and $n_2/(1-z_E)$ for $z > z_E$, respectively. Consequently, the heat Q evolved in reactions [5] and [6] is given by $(n_1/n_E)\Delta_{fus}H^0$ and $[n_2/(1-z_E)]\Delta_{fus}H^0$, respectively, where $\Delta_{fus}H^0$ is the molar heat of fusion of the eutectic. Then, it can be concluded that the ratios Q/n_1 and Q/n_2 must be independent of z for $z < z_E$ and $z > z_E$, respectively. In Table 3 are listed the experimental values of Q, Q/n_1, and Q/n_2 calculated from DSC traces registered from samples with compositions z in the range 0.369–0.975. It can be seen that Q/n_1 and Q/n_2 are almost constant for $0.369 \leq z \leq 0.857$ and $z \geq 0.909$, respectively, which validate the eutectic reactions proposed above. Their average values are 19.56(15) and 190(7) kJ mol^{-1}, respectively. From these results it can be deduced that z_E lies between 0.857 and 0.909. From the two relationships between $\Delta_{fus}H^0$, Q/n_1, Q/n_2, and z_E as given above, the average values calculated for z_E and $\Delta_{fus}H^0$ are 0.906(5) and 17.7(5) kJ mol^{-1}, respectively. These results allow us to establish the phase equilibria diagram for the binary system $K_3La_2(NO_3)_9$–KNO_3 (Fig. 12).

According to the decomposition process of $K_2La(NO_3)_5 \cdot 2H_2O$ described in Section IV, it is clear that the first stage leads to the mixture of phases $[(1-z)K_3La_2(NO_3)_9, zKNO_3]$ with $z = 0.5$ (see chemical reaction [1]), which subsequently gives a mixture of liquid eutectic and $K_3La_2(NO_3)_9$ in excess from 250°C. As a consequence, above this temperature the proportion of $K_3La_2(NO_3)_9$ in the mixture is lower than in the initial solid mixture. It is the reason why the intensity of the diffraction lines of its powder pattern decreases suddenly at $\sim$ 250°C (Fig. 3 and Section IV).

IX. STRUCTURAL CHARACTERIZATION OF $LaONO_3 \cdot \frac{1}{3}KNO_3$ AND CUBIC La_2O_3

Some crystallographic characterizations of the two new phases $LaONO_3 \cdot \frac{1}{3}KNO_3$ and cubic La_2O_3 identified in the course of the study have been carried out by X-ray powder diffraction.

$LaONO_3 \cdot \frac{1}{3}KNO_3$

Attempts to solve *ab initio* the crystal structures of the two polymorphic phases α-$LaONO_3 \cdot \frac{1}{3}KNO_3$ and β-$LaONO_3 \cdot \frac{1}{3}KNO_3$ from X-ray powder diffraction data were not fully successful, even though the quality of the data was satisfactory (see Fig. 7). It is clear that with such a chemical formula and $Z = 4$, involving a noninteger number of "KNO_3" units in the cell, the crystal structure determination cannot be easy. It is also likely that the unit cell suggested by DICVOL91 is a subcell and that a substructure model should thus be evoked, though no substructure reflection was identified in the X-ray diffraction pattern.

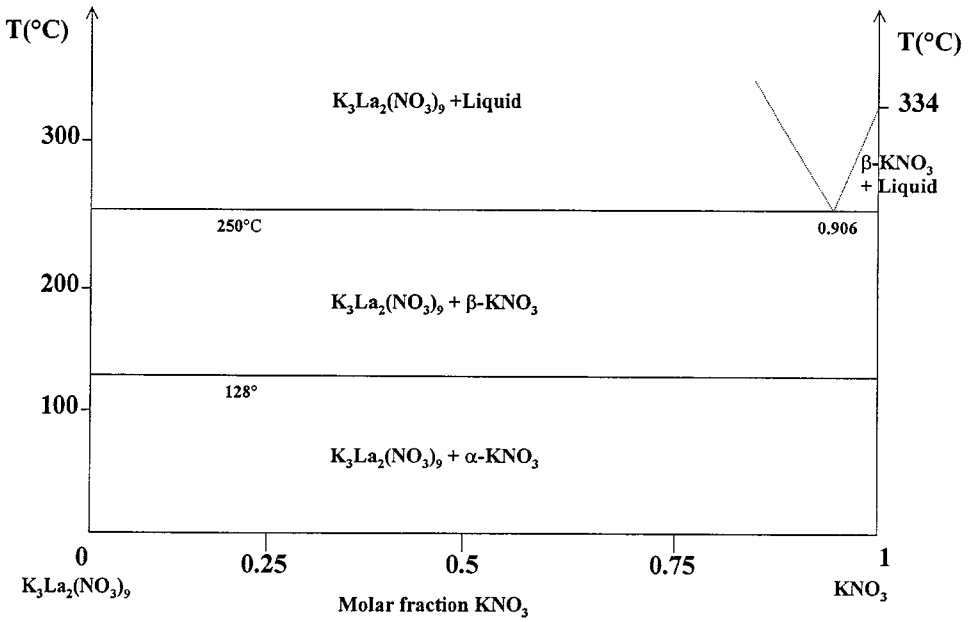

FIG. 12. $K_3La_2(NO_3)_9$–KNO_3 phase diagram (the dotted lines are assumed to be the liquidus borders).

However, from the structure study, assuming space group *I*222, some reasonable fragments were suggested. For this study precise data were collected at room temperature for the α phase (Cu$K\alpha_1$ radiation, step size: 0.02°2θ, angular range: 6°–150°2θ, counting time: 29 s step^{-1}) and at 390°C for the β phase (Cu$K\alpha_{1,2}$ radiation, step size: 0.02°2θ, angular range: 5°–100°2θ, counting time: 31 s step^{-1}). Patterson maps were calculated from the structure factor amplitudes extracted by an iterative pattern decomposition algorithm, from which the heavy atoms positions were derived (0.5, 0.5, 0.7014 for α-$LaONO_3 \cdot \frac{1}{3}KNO_3$ and 0.5, 0.5, 0.7032 for β-$LaONO_3 \cdot \frac{1}{3}KNO_3$). Although successive Fourier maps were performed to locate the remaining atoms, only one oxygen atom position was found (0.0, 0.5, 0.7297 for α-$LaONO_3 \cdot \frac{1}{3}KNO_3$ and 0.0, 0.5, 0.7600 for β-$LaONO_3 \cdot \frac{1}{3}KNO_3$). These results must be analyzed with caution. However, it is interesting to note that the identified oxygen atom is linked to the La atom, from which results a layer with the basic formula $(LaO)_n^{n+}$. This cationic layer is similar to that observed in the oxide salts with the general formula $(LnO)_nX_n$ (X = NO_3, Cl, Br, SO_4) (9, 21–23).

Cubic La_2O_3

The cubic phase was prepared from $K_2La(NO_3)_5 \cdot 2H_2O$, decomposed under vacuum at 540°C (see Section IV). At this temperature, the oxide is mixed with a liquid (see Section VIII). Data were collected *in situ* at this temperature using Bragg–Brentano geometry (Cu$K\alpha_{1,2}$). Patterns were scanned with a step size of 0.05°(2θ) over the angular range 20°–95°(2θ) with a counting time of 37 s step^{-1}. Although the quality of the data is low and the diffraction lines are extremely broad, the Rietveld refinement of the structure, with the program FULLPROF (24), was performed with the unit cell parameter and the atomic positions of the isostructural cubic oxide Tm_2O_3 (space group *Ia*3) as initial structure model (25). The final refinement involved the following parameters: 4 atomic coordinates, 1 scale factor, 2 isotropic atomic displacement factors (the two La atoms were constrained to have the same thermal parameter), 1 zero-point parameter, 1 cell parameter, 3 half-width parameters. Four coefficients were used to describe the functional dependence of the background. The refined cell parameter was $a = 11.414(3)$ Å and the final Rietveld plot is shown in Fig. 13. It can be seen that, due to the experimental conditions used, the diffraction lines of the sample holder made of Ni sponge are also observed. Consequently, the Rietveld refinement was carried out simultaneously for the two phases, Ni and cubic La_2O_3. The final fit corresponds to satisfactory crystal structure model indicators (R_F = 7.59% and $R_B = 9.26\%$) and profile factors ($R_p = 11.2\%$ and $R_{wp} = 14.4\%$). The atomic coordinates are given in Table 4.

The structure of cubic La_2O_3 belongs to the C-type structure of the classification of rare-earth sesquioxides established by Goldschmidt (26). According to Caro (27), this structure can also be described from an arrangement of OLa_4 tetrahedra sharing corners. Moreover, the

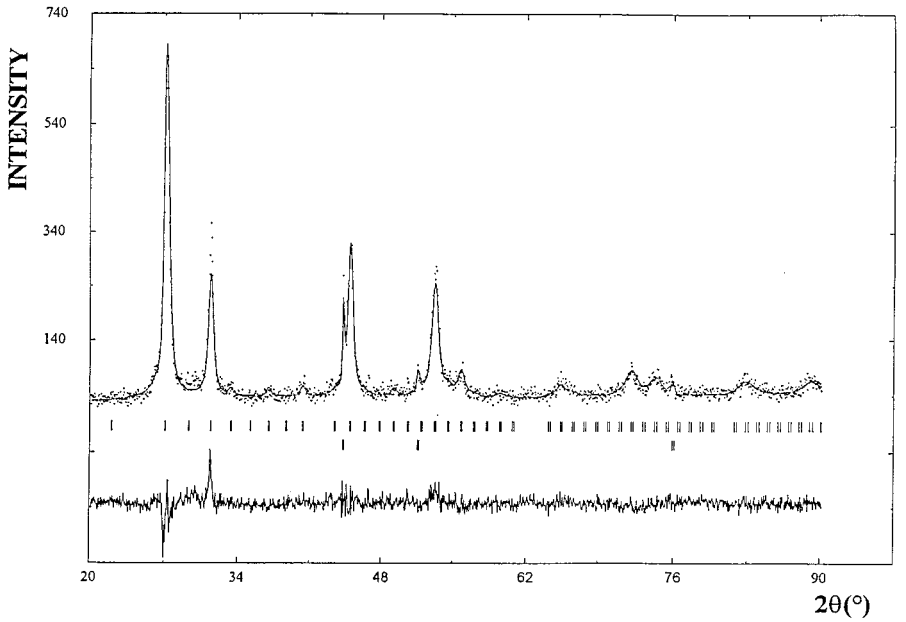

FIG. 13. Final Rietveld plot for cubic La_2O_3. The upper traces show the observed data as dots, while the calculated pattern is shown by solid lines. The vertical markers show positions calculated for Bragg reflections for La_2O_3 (top) and Ni (bottom). The lower trace is the difference between observed and calculated patterns.

extrapolation of the linear relationship between the unit cell dimensions and the cation radius for the C-type cubic rare-earth oxide structures (from Nd and Lu) [Fig. 3 in Ref. (28)] gives a parameter 11.434 Å for the radius of La atom (1.14 Å). This calculated value agrees well with the value 11.414 Å reported in the present study.

It should be noted that cubic La_2O_3 has been observed during the synthesis of lanthanum orthosilicates at 1600°C (29). However, the formation at low temperature of metastable cubic La_2O_3 from thermal decomposition of precursors was questionable. Indeed, Roth and Schneider (28) stated that *this question cannot be answered unless a method is found to produce La_2O_3 by decomposing a lanthanum compound below 500°C*. The present study clearly demonstrates that $K_2La(NO_3)_5 \cdot 2H_2O$ is such a precursor, since cubic La_2O_3 is formed under vacuum from 450°C.

TABLE 4
Atomic Coordinates and Atomic Displacement Parameters for Cubic La_2O_3 at 540°C [a=11.414(3) Å]

Atom	x	y	z	B_{iso} (Å^2)
Lal	0.25	0.25	0.25	0.7(2)[a]
La2	− 0.017(1)	0.0	0.25	0.7(2)
O	0.392(1)	0.161(5)	0.352(8)	0.6(9)

[a] SD in parentheses.

X. SUMMARY

TDXD, TG, and DSC studies have shown that the thermal decomposition of $K_2La(NO_3)_5 \cdot 2H_2O$ and $K_2La_2(NO_3)_9$ are very complex, with the occurrence of new intermediate compounds. To describe completely the successive stages of these decompositions, it has been necessary to establish the phase relationships in the binary systems $LaONO_3$–KNO_3 and $K_3La_2(NO_3)_9$–KNO_3. The main results arising from these studies can be summarized as follows:

1. The new phase $K_3La_2(NO_3)_9$ is a decomposition product of $K_2La(NO_3)_5 \cdot 2H_2O$. It belongs to the family of the cubic compounds with the general formula $M_3Ln_2(NO_3)_9$ (M = alkaline metal or ammonium ion).

2. The chemical formula of the new intermediate phase identified in the decomposition process of the two precursors, initially denoted X, has been elucidated from the establishment of the phase equilibrium diagram $LaONO_3$–KNO_3, i.e., $LaONO_3\ \frac{1}{3}KNO_3$. This compound has also been obtained independently from a peritectic reaction between a liquid rich in KNO_3 and β-$LaONO_3$. This new compound undergoes a polymorphic transformation at 310°C. The crystal symmetry of these two phases is orthorhombic and the crystal structure is likely derived from the structure of $LaONO_3$, but with species such as "KNO_3" located between the layers $(LaO)_n^{n+}$.

TABLE 5
Successive Stages of the Decomposition of $K_2La(NO_3)_5 \cdot 2H_2O$ under Nitrogen

Stage	Transformation[a]	Temperature range (°C) (TDXD)
1	$2K_2La(NO_3)_5 \cdot 2H_2O_{(s)} \downarrow K_3La_2(NO_3)_{9(s)} + KNO_{3(am)} + 4H_2O_{(g)}$	90–100
2	$KNO_{3(am)} \downarrow \beta\text{-}KNO_{3(s)}$	128
3	$K_3La_2(NO_3)_{9(s)} + \beta\text{-}KNO_{3(s)} \downarrow 0.104[K_3La_2(NO_3)_9 \cdot 9.62KNO_3]_{(l)} + 0.896K_3La_2(NO_3)_{9(s)}$	250
4	$0.896K_3La_2(NO_3)_{9(s)} \downarrow 1.792\alpha\text{-}LaONO_3 \cdot \frac{1}{3}KNO_{3(s)} + 2.09KNO_{3(l)} + (NO, NO_2, O_2)_{(g)}$	330–340
5	$1.792\alpha\text{-}LaONO_3 \cdot \frac{1}{3}KNO_{3(s)} \downarrow 1.792\beta\text{-}LaONO_3 \cdot \frac{1}{3}KNO_{3(s)}$	350
6	$1.792\beta\text{-}LaONO_3 \cdot \frac{1}{3}KNO_{3(s)} + 0.104[K_3La_2(NO_3)_9 \cdot 9.62KNO_3]_{(l)} + 2.09KNO_{3(l)} \downarrow La_2O_{3(c)} + (NO, NO_2, O_2, \text{“}KNO_3\text{”})_{(g)}$	400–420
7	$La_2O_{3(c)} \downarrow La_2O_{3(h)}$	485–540

[a]am, amorphous; c, cubic; h, hexagonal.

3. In the binary phase equilibrium diagram $K_3La_2(NO_3)_9$–KNO_3, a eutectic was found to be located at the KNO_3 molar fraction 0.906 and 250°C.

4. $K_2La(NO_3)_5 \cdot 2H_2O$ and $K_3La_2(NO_3)_9$ are two precursor materials of cubic La_2O_3.

5. The oxide nitrate $LaONO_3$ undergoes a polymorphic transformation at 167°C. The two varieties crystallize with tetragonal symmetry.

The successive stages of the complex thermal decomposition of $K_2La(NO_3)_5 \cdot 2H_2O$ under nitrogen and

TABLE 6
Successive Stages of the Decomposition of $K_3La_2(NO_3)_9$ under Vacuum

Stage	Transformation[a]	Temperature range (°C) (TDXD)
1	$K_3La_2(NO_3)_{9(s)} \downarrow 2\alpha\text{-}LaONO_3 \cdot \frac{1}{3}KNO_{3(s)} + \frac{7}{3}KNO_{3(am)} + (NO, NO_2, O_2)_{(g)}$	215–300
2	$\frac{7}{3}KNO_{3(am)} \downarrow \frac{7}{3}KNO_{3(l)}$	334
3	$2\alpha\text{-}LaONO_3 \cdot \frac{1}{3}KNO_{3(s)} \downarrow 2\beta\text{-}LaONO_3 \cdot \frac{1}{3}KNO_{3(s)}$	350
4	$2\beta\text{-}LaONO_3 \cdot \frac{1}{3}KNO_{3(s)} + \frac{7}{3}KNO_{3(l)} \downarrow La_2O_{3(c)} + (NO, NO_2, O_2, \text{“}KNO_3\text{”})_{(g)}$	380–400

[a] am, amorphous; c, cubic.

$K_3La_2(NO_3)_9$ under vacuum are summarized in Tables 5 and 6, respectively. When the decomposition of $K_2La(NO_3)_5 \cdot 2H_2O$ is performed under vacuum, stages 3 and 4 (Table 5) are superimposed and the cubic–hexagonal transformation of La_2O_3 is only partial at 800°C. It is worth noting that pure La_2O_3 is the final product of the decompositions. Consequently, it must be concluded that the liquid phases [mixture ($K_3La_2(NO_3)_9$,KNO_3) above 250°C or liquid KNO_3 above 334°C] are totally decomposed into gaseous products according to complex mechanisms (30).

To conclude, the present study shows the importance of obtaining different types of experimental evidence, through the use of complementary techniques as TG, DSC, XRD, TDXD, and optical microscopy, to interpret complex decomposition mechanisms in solid materials involving the formation of liquid phases. Such a statement was recently clearly expressed by Galwey (31). Indeed, the decomposition process of $K_2La(NO_3)_5 \cdot 2H_2O$ cannot be explained from only TG analysis, since it suggests the formation of the anhydrous phase $K_2La(NO_3)_5$ instead of the mixture [$K_3La_2(NO_3)_9$, KNO_3] pointed out from TDXD. Another example is the formation of a eutectic between $K_3La_2(NO_3)_9$ and KNO_3, which was demonstrated by using both DSC measurements and microscopic examination. It should also be noted that the phase relationships in the system $LaONO_3$–KNO_3 have been established from the complementary results of DSC and TDXD. Clearly, the mechanism of the decomposition of $K_2La(NO_3)_5 \cdot 2H_2O$ is totally different from that reported by Karppinen *et al.* (2). Finally, the present study demonstrates that special attention must be paid to phenomena involving partial melting of the sample due to the formation of a eutectic or a liquid product, which can play a peculiar role in the thermal decomposition process.

ACKNOWLEDGMENTS

One of the authors (A.-E. Gobichon) is indebted to the Conseil Régional de Bretagne for financial support.

REFERENCES

1. N. Audebrand, J. P. Auffrédic, M. Louër, N. Guillou, and D. Louër, *Solid State Ionics* **84,** 323 (1996).
2. M. Karppinen, P. Kyläkoski, L. Niinistö, and C. Rodellas, *J. Therm. Anal.* **35,** 347 (1980).
3. A. K. Molodkin, Z. K. Odinets, and O. Vargas Ponse, *Russ. J. Inorg. Chem.* **21,** 1425 (1976).
4. A. G. Dryuchko and V. Shevchuk, *Russ. J. Inorg. Chem.* **30,** 1132 (1985).
5. N. Audebrand, J. P. Auffrédic, and D. Louër, *Thermochim. Acta* **293,** 65 (1997).
6. N. Audebrand, J. P. Auffrédic, and D. Louër, *J. Solid State Chem.* **132,** 361 (1997).
7. C. A. Ebbers, L. D. Deloach, M. Webb, D. Eimerl, S. P. Velsko, and D. A. Keszler, *IEEE J. Quantum Electron.* **29,** 497 (1993).
8. B. Eriksson, L. O. Larsson, L. Niinistö, and J. Valkonen, *Acta Chem. Scand. A* **34,** 567 (1980).
9. A.-E. Gobichon, J. P. Auffrédic, and D. Louër, *Solid State Ionics* **93,** 51 (1997).
10. J. Plévert, J. P. Auffrédic, M. Louër, and D. Louër, *J. Mater. Sci.* **24,** 1913 (1989).
11. A. Boultif and D. Louër, *J. Appl. Crystallogr.* **24,** 987 (1991).
12. C. K. Fair, "MolEN: An Interactive Intelligent System for Crystal Structure Analysis." Enraf-Nonius, Delft, 1990.
13. E. L. Charsley, *J. Therm. Anal.* **40,** 1399 (1993).
14. International Centre for Diffraction Data, Newtown Square, PA.
15. N. Guillou, J. P. Auffrédic, and D. Louër, *Acta Crystallogr. C* **51,** 1032 (1995).
16. M. R. Anderson, G. T. Jenkin, and J. W. White, *Acta Crystallogr. B* **33,** 3933 (1977).
17. A.-E. Gobichon, J. P. Auffrédic, and D. Louër, *J. Alloys Compd.* **275–277,** 130 (1998).
18. A. G. Vigdorchik, Yu. A. Malinovskii, A. G. Dryuchko, and I. A. Verin, *Sov. Phys. Crystallogr.* **36**, 789 (1991).
19. A. D. Mighell, C. R. Hubbard, and J. KL. Stalick, "A FORTRAN Program for Crystallographic Data Evaluation," Natl. Bur. Stand. Tech. Note 1141 (1981). (NBS*AIDS83 is an expanded version of NBS*AIDS80). U.S.
20. International Centre for Diffraction Data, NIST CDF database, Newtown Square, PA.
21. L. H. Brixner and E. P. Moor, *Acta Crystallogr. C* **39**, 1316 (1983).
22. I. Mayer, S. Zolotov, and F. Kassierer, *Inorg. Chem.* **4,** 1637 (1965).
23. S. Zhukov, A. Yatsenko, V. Chernyshev, V. Trunov, E. Tserkovnaya, O. Antson, J. Hölsa, P. Baulés, and H. Schenk, *Mater. Res. Bull.* **32,** 43 (1997).
24. J. Rodriguez Carvajal, *in* "Collected Abstracts of Powder Diffraction Meeting," p. 127. Toulouse, 1990.
25. H. Ishibashi, K. Shimomoto, and K. Nakahigashi, *J. Phys. Chem. Solids* **55,** 809 (1994).
26. V. M. Goldschmidt, *Geochem. Vert.-Ges. D. EL.* IV, V, Videnskapsselsk, Skr., 5,7, Oslo, (1925).
27. P. E. Caro, *J. Less-Common Met.* **16,** 367 (1968).
28. R. S. Roth and S. J. Schneider, *J. Res. Natl. Bur. Stand.* **64A,** 309 (1960).
29. J. Felsche, *Naturwissenschatten* **56,** 212 (1969).
30. C. C. Addison and N. Logan, *Adv. Inorg. Chem. Radiochem.* **6,** 72 (1964).
31. A. Galwey, *Pure Appl. Chem.* **67,** 1809 (1995).